catalysts

MDPI

Article

Gel-Type and Macroporous Cross-Linked Copolymers Functionalized with Acid Groups for the Hydrolysis of Wheat Straw Pretreated with an Ionic Liquid

Giulia Lavarda [1,2], Silvia Morales-delaRosa [2,*], Paolo Centomo [1,*], Jose M. Campos-Martin [2], Marco Zecca [1] and Jose L. G. Fierro [2]

[1] Dipartimento di Scienze Chimiche, Università di Padova, via Marzolo 1, I-35131 Padua, Italy
[2] Sustainable Energy and Chemistry Group. Instituto de Catálisis y Petroleoquímica, CSIC, Marie Curie, 2, Cantoblanco, 28049 Madrid, Spain
* Correspondence: smorales@icp.csic.es (S.M.-d.); paolo.centomo@unipd.it (P.C.)

Received: 12 July 2019; Accepted: 6 August 2019; Published: 8 August 2019

Abstract: Several sulfonated cross-linked copolymers functionalized with hydroxyl and carboxylic groups have been synthesized. The amount of the cross-linking monomer was tailored (from 4% up to 40%) to tune the resulting micro- and nano-morphologies, and two types of catalysts, namely, gel-type and macroreticular catalysts, were obtained. These copolymers were employed in the catalytic hydrolysis of wheat straw pretreated in 1-ethyl-3-methylimidazolium acetate to obtain sugars. Remarkably, the presence of additional oxygenated groups enhances the catalytic performances of the polymers by favoring the adsorption of β-(1,4)-glucans and makes these materials significantly more active than an acidic resin bearing only sulfonic groups (i.e., Amberlyst 70). In addition, the structure of the catalyst (gel-type or macroreticular) appears to be a determining factor in the catalytic process. The gel-type structure provides higher glucose concentrations because the morphology in the swollen state is more favorable in terms of the accessibility of the catalytic centers. The observed catalytic behavior suggests that the substrate diffuses within the swollen polymer matrix and indirectly confirms that the pretreatment based on dissolution/precipitation in ionic liquids yields a substantial enhancement of the conversion of lignocellulosic biomass to glucose in the presence of heterogeneous catalysts.

Keywords: heterogeneous catalysts; ionic liquid; lignocellulosic biomass; acidic resin catalysts

1. Introduction

Sustainable energy is increasingly being applied to all social, economic and political fields worldwide. The European Union (EU) has a political objective to decarbonize its economy by 2050 and reduce 80%−95% of its greenhouse gas (GHG) emissions [1,2].

In addition, market requirements are trending towards an ecological compromise, and society is increasingly becoming aware of the need to consume products that have been obtained through processes with minimized environmental impacts. As a result, the use of bioproducts, renewable energy [3] and biorefineries is constantly expanding to various industries, such as the chemical, pharmaceutical, paper and food industries, as well as others.

The total amount of lignocellulosic biomass produced in the EU-28 is calculated to be 419 Mt, among which wheat is the main contributor (155 Mt, 37%). Thus, these residues are highly suitable raw materials for both producing second-generation biofuels and preparing high value-added compounds in the EU [4].

The transformation of lignocellulosic biomass into valuable chemicals requires, almost inevitably, a previous treatment (physical, chemical, biochemical, biological or a combination of them) of the

substrate [5]. In this way, the particle size can be reduced, the porosity can be improved, and the crystallinity of the cellulose can be altered. After fractioning its main components, e.g., cellulose, hemicellulose and lignin, biomass can be converted into a wide variety of industrial products, such as biofuels, biomaterials, cellulose pulps, cellulose nanofibers, oligosaccharides and a large number of by-products, in addition to lignin derivatives.

Numerous studies have shown ionic liquids (ILs) to be effective at solubilizing lignocellulosic biomass, allowing for subsequent regeneration by precipitation with anti-solvents. Depending on the anti-solvent used, it is possible to achieve selective precipitation and separate the lignocellulosic biomass into its main components [6–14]. Among the most commonly employed ILs, 1-ethyl-3-methylimidazolium acetate ([EMIM]OAc) holds a privileged position due to its physico-chemical properties.

The acid hydrolysis of the polysaccharide fractions of lignocellulosic biomass, which leads to monosaccharides that can be converted into fine chemicals or platform molecules used for industrial applications, can be performed in the presence of enzymes, homogeneous catalysts or heterogeneous catalysts [15–21]. During the last few years, increasing attention has been focused on the heterogeneous approach, which leads to several advantages in terms of the process design and plant costs [22–25]. Some of us have investigated using resins as catalysts or scaffolds in material chemistry [26–30]. These resins could be more advantageous materials than the most commonly employed materials used for the acid hydrolysis of lignocellulosic biomass (e.g., zeolites, carbon and hybrid materials), especially due to their structural and functional versatility and stability in reaction media. In fact, the morphology and chemical properties of these resins can be easily tuned by modifying the nature and amount of structural, cross-linking and functional monomers used [31–33].

The presence of additional polar groups in combination with sulfonic groups in carbon-based materials clearly enhances the hydrolysis of cellulose [34–37] by favoring the adsorption of β-(1,4)-glucans. This effect was observed also in other supports, such as silica and resins [38–40]. However, the effect on the catalytic performances of the polar group amount and of the synergy between the presence of additional acid groups and the morphology of the polymer matrix has not yet been studied.

In this work, we describe the design and synthesis of several novel cross-linked copolymers, as well as the ability of these copolymers to catalyze the acid hydrolysis of wheat straw pretreated with [EMIM]OAc. For these catalysts, the amount of the cross-linking monomer has been tailored to tune the morphology of the materials from a gel-type matrix to a macroreticular structure. Moreover, the chemical properties of the supports have been controlled by decorating the polymers with carboxylic and hydroxyl groups. The percentage of the functional monomer was adjusted to study the effect of the number of polar groups on the performance of the catalyst.

2. Results and Discussion

2.1. Synthesis of the Catalysts

Two copolymers containing 2-acrylamido-2-methyl-1-propanesulfonic acid (AMPS), 2-hydroxyethyl methacrylate (HEMA) and ethylene dimethacrylate (EDMA) and four copolymers containing AMPS, methacrylic acid (MAA) and EDMA were prepared by free radical polymerization using N,N-Dimethylformamide (DMF) as the solvent.

For both the AHE (AMPS-HEMA-EDMA) and AME (AMPS-MAA-EDMA) polymers (see Sections 3.2 and 3.3 of this work), the ratio of HEMA or MAA to AMPS was tuned from 1:2 to 1:3 to obtain materials with different amounts of polar groups. In the case of the AHE catalysts, the molar amount of the cross-linking monomer (EDMA) was established to obtain gel-type textures. For the AME materials, the molar percentage of EDMA was varied from 4% to 40%, and two kinds of catalysts were obtained, i.e., gel-type structures and rigid macroreticular resins. The notations AHE Y-X and AME Y-X, where Yand X are the nominal molar ratios of AMPS and EDMA, respectively, will be used henceforward to refer to the polymer materials. The expected chemical structures of the AHE and AME materials are reported in Figures 1 and 2.

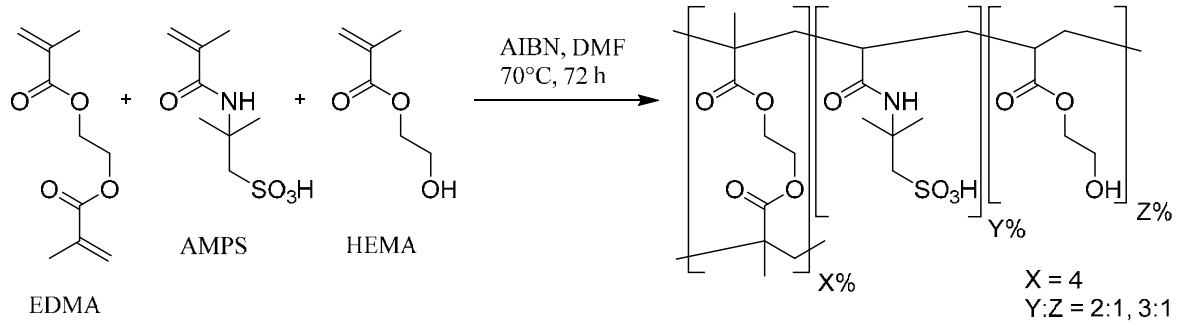

Figure 1. Chemical structure of the AHE copolymers.

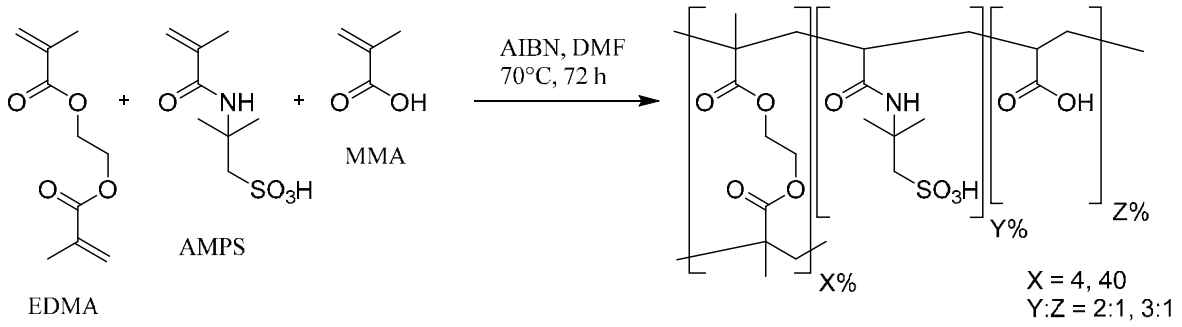

Figure 2. Chemical structure of the AME copolymers.

2.2. Elemental Analysis and Cation Exchange Capacity (CEC) of the Catalysts

The elemental analysis and determination of the cation exchange capacity (CEC) by back-titration confirmed the composition of the synthetized AME and AHE materials (Tables 1 and 2). Slight differences between the expected elemental composition (calculated from the composition of the monomer mixtures) and the experimental results may be due to the incomplete polymerization of the monomers or the presence of moisture in the materials. As a matter of fact, the presence of a substantial amount of water in acrylic resins is well known, particularly in the case of polar monomers, which makes quite reliable the hypothesis of the presence of water in the AHE and AME materials. Regarding the cation exchange capacity of the AME and AHE catalysts, back-titration pointed out that the actual CEC of the materials is somewhat lower than the nominal CEC (calculated from the AMPS molar content), although the results appear in good agreement.

Table 1. The expected molar composition of the AHE materials.

		χ (%)			Weight Ratios (%)				CEC
		AMPS	**HEMA**	**EDMA**	**C**	**H**	**N**	**S**	**(mmol H^+/g)**
AHE 64-4	Experimental	-	-	-	45.36	6.56	4.75	10.29	3.12
	Theoretical [1]	64	32	4	45.12	6.06	4.95	11.34	3.48 [2]
AHE 72-4	Experimental	-	-	-	43.94	6.49	5.27	11.53	3.47
	Theoretical [1]	72	24	4	43.87	6.59	5.35	12.26	3.78 [2]

[1] Excludes the presence of contaminants; [2] cation exchange capacity (CEC) was calculated from the AMPS content.

The explanations for these discrepancies are the same as those mentioned in the elemental analysis. In the case of the AME polymers, the possibility that the CEC values were underestimated due to the re-acidification of the more accessible carboxylic groups during the titration must also be considered.

Table 2. The expected molar composition of the AME materials.

		χ (%)			Weight Ratios (%)				CEC (mmol H^+/g)
		AMPS	**MAA**	**EDMA**	**C**	**H**	**N**	**S**	
AME 64-4	Experimental	-	-	-	43.4	6.42	5.08	10.75	5.49
	Theoretical [1]	64	32	4	44.01	6.48	5.23	12.21	5.71 [2]
AME 72-4	Experimental	-	-	-	42.53	6.42	5.45	11.56	5.3
	Theoretical [1]	72	24	4	43.23	6.44	5.67	12.98	5.4 [2]
AME 40-40	Experimental	-	-	-	50.82	6.65	3.01	6.3	2.99
	Theoretical [1]	40	20	40	50.8	6.74	3.12	7.15	3.34 [2]
AME 45-40	Experimental	-	-	-	49.97	6.65	3.36	6.66	2.98
	Theoretical [1]	45	15	40	50.19	6.71	3.4	7.78	3.24 [2]

[1] Excludes the presence of contaminants; [2] CEC was calculated from the AMPS content.

2.3. FTIR Spectroscopy of Catalysts

From the FTIR spectra of the AHE materials (Figure 3), the broad band at approximately 3500 cm^{-1} is due to the N-H stretching of the acrylamide moiety (AMPS), the O-H stretching of the hydroxyl group of HEMA and the sulfonic group of AMPS and the water contribution. The group of bands at 2858–2964 cm^{-1} can be attributed to the stretching of C-H bonds. The signal corresponding to the C=O stretching of the ester group of HEMA and EDMA can be observed at 1732 cm^{-1}. The signal at 1644–1647 cm^{-1} can be ascribed to the stretching of the carbonyl groups of the acrylamide moiety (amide I band), whereas the weak signal at 1557 cm^{-1} is due to N-H bending (amide II band). The stretching of the C-N bond of the acrylamide group produces a signal at 1408 cm^{-1}. The strong bands at 1262 cm^{-1} and 1097–1099 cm^{-1} can be attributed to the asymmetric and symmetric stretching of the sulfonic group of AMPS, respectively, whereas the band at 1024–1025 cm^{-1} can be ascribed to the asymmetric O-C-C stretching of HEMA and EDMA. The strong band at 802–803 cm^{-1} is due to the out-of-plane wagging vibration of the N-H bonds of the primary amide group. Finally, it is possible to exclude the presence of a significant amount of unreacted C=C double bonds, due to the lack of signals at 1637 and 1610 cm^{-1}, which are expected for alkenes conjugated to carbonyl groups [41].

In the FTIR spectra of the AME materials (Figure 4), the N-H stretching of the acrylamide moiety and the O-H stretching of the sulfonic group in the AMPS monomer (as well as the water contribution) generate the broad band at approximately 3500 cm^{-1}. The C=O stretching of the ester group in the cross-linking monomer produces a band at 1725–1734 cm^{-1}. The C=O stretching of the acrylamide moiety generates a peak at 1652–1646 cm^{-1} (amide I band), whereas N-H bending is associated with a weak signal at 1557–1555 cm^{-1}. The signal at 1400 cm^{-1} is associated with the stretching of C-N. In addition, the asymmetric and symmetric stretching of the sulfonic group of AMPS produces two intense signals at 1261 cm^{-1} and 1101–1105 cm^{-1}, respectively, whereas the coupled C-C(=O)-O and O-C-C vibrations produce a band at 1035 cm^{-1} and contribute to the strong signal at 1261 cm^{-1}. The strong signal at 800–802 cm^{-1} is related to the out-of-plane wagging of the N-H bond in AMPS. As observed for the AHE resins, the lack of bands related to C=C stretching confirms the absence of appreciable amounts of unreacted monomers.

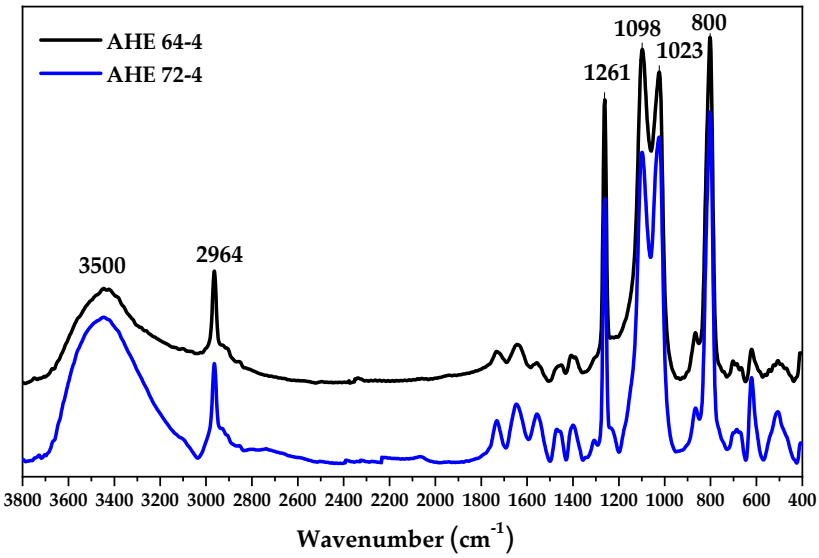

Figure 3. FTIR absorption spectra of the AHE catalysts.

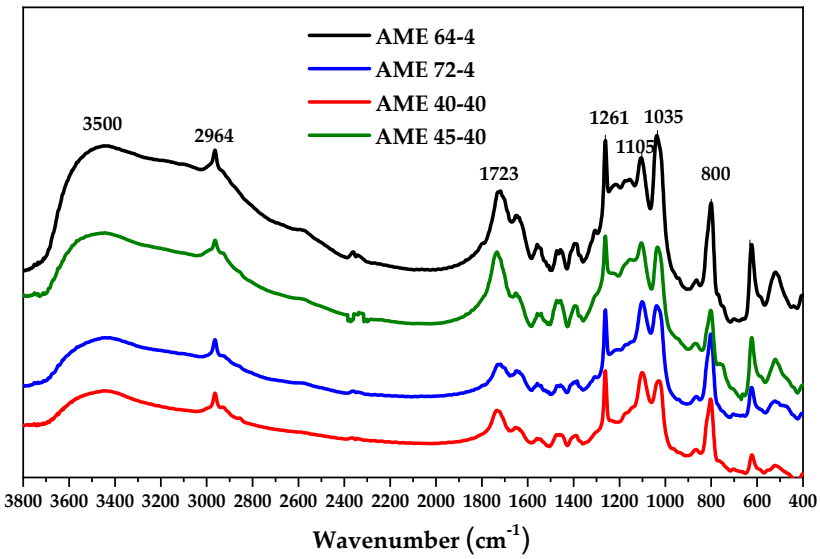

Figure 4. FTIR absorption spectra of the AME catalysts.

2.4. X-Ray Diffraction Analysis of the Wheat Straw Samples

The X-ray diffraction pattern of the untreated wheat straw (Figure 5) shows the characteristic peaks of the raw cellulose crystalline structure, although the signals are slightly weaker and broader with respect to the pure commercial cellulose. This effect can be attributed to the presence of amorphous components, such as hemicellulose and lignin, which do not have ordered structures. The strong peak at 23° corresponds to the diffraction generated by the (200) plane, whereas the wide peak between 15° and 17° represents the combination of the two reflections corresponding to (110) and ($1\bar{1}0$). The combined signal centered at 34° consists of several overlapping signals, among which is the signal generated from the (004) plane [42].

The X-ray diffraction pattern of the IL-treated wheat straw shows important changes with respect to the original sample (Figure 5). The intensity of the diffractogram is very low, indicating a clear loss in the initial crystallinity. Only a low intense and broad peak is detected at approximately 23°, which indicates the incipient formation of cellulose II, a structure that can appear in dissolved/regenerated cellulose.

This behavior has already been reported in previous works published by us and other authors using different samples of lignocellulosic biomass after pretreatment with ILs [17,21,43].

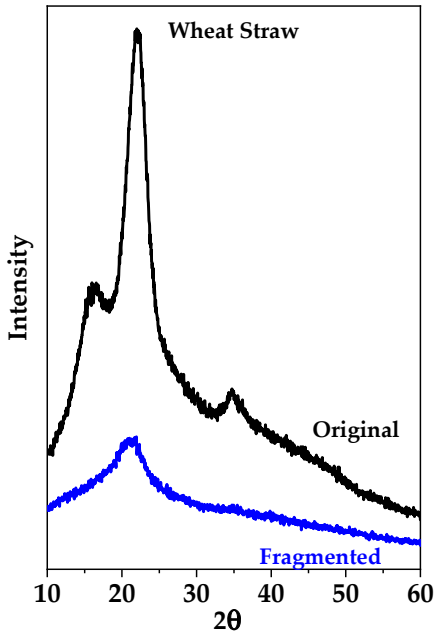

Figure 5. XRD characterization of the original wheat straw and solid fraction (rich in sugars) after pretreatment with [EMIM]OAc.

2.5. SEM Analysis of the Wheat Straw Samples

From the SEM micrographs of the original raw wheat straw samples, which were obtained at different magnifications, a structure consisting of vascular bundles forming hollows along small fragments (0.250 μm) is observed (Figure 6). In contrast, the treated sample shows a dramatic change in the structure and morphology of the material (Figure 7). These structural changes have been previously described for cellulose or lignocellulosic biomass samples treated with [EMIM]OAc and other ILs [21,39]. The surface of the pretreated solid (Figure 7) appears to be more porous than in the untreated wheat straw, making the biomass more susceptible to hydrolysis. The presence of remaining fragments of raw wheat straw (Figure 7) may be due to incomplete dissolution of the biomass, which allowed for the partial retention of the initial structure.

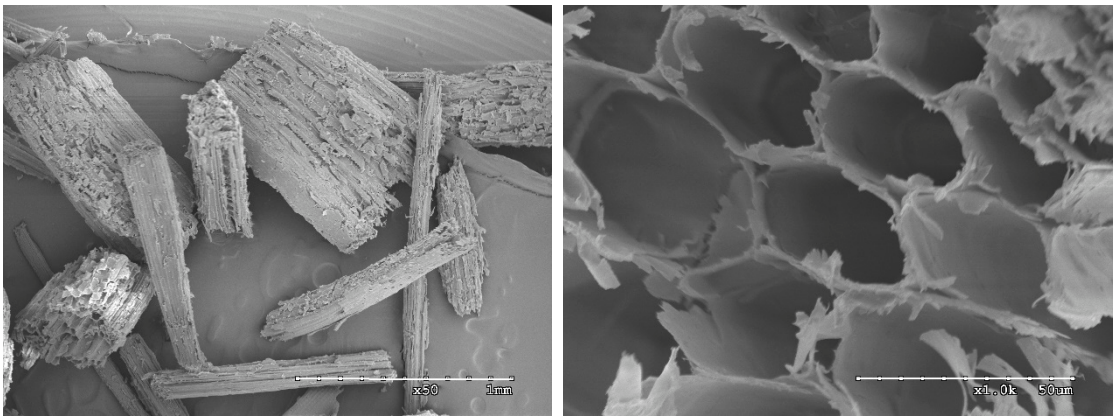

Figure 6. SEM micrographs of the raw wheat straw.

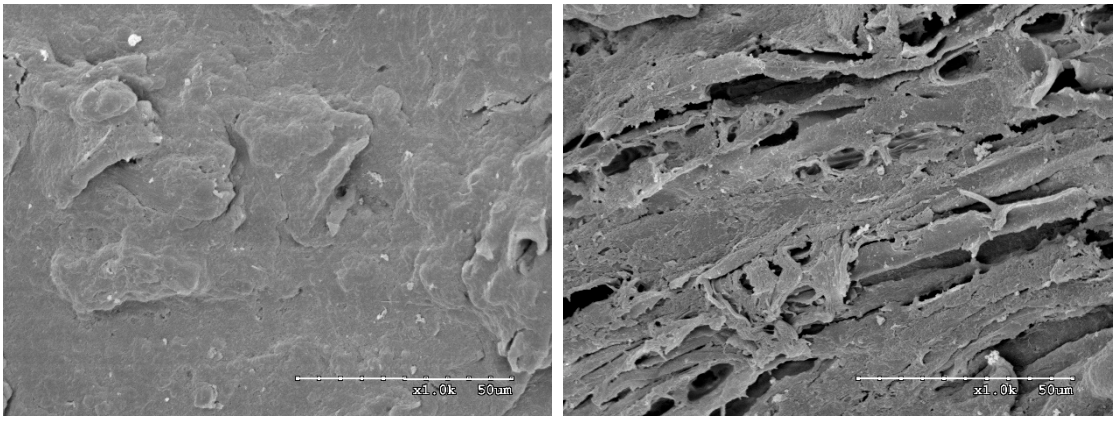

Figure 7. SEM micrographs of the wheat straw after dissolution in [EMIM]OAc (at 105 °C) and precipitation with acetone:water (1:1).

These results agree with the data obtained from X-ray diffraction, as both techniques clearly indicate that the original structure of the wheat straw is altered after pretreatment with [EMIM]OAc and subsequent fractional precipitation in the presence of acetone:water (1:1).

2.6. FTIR Spectroscopy of the Wheat Straw Samples

The changes in the composition of the wheat straw samples after pretreating with [EMIM]OAc were studied by attenuated total reflectance-Fourier transform infrared spectroscopy (ATR-FTIR). The region between 1800 and 850 cm^{-1} of the spectra is quite complex, and many peaks related to the main biomass component can be detected, allowing for changes in the composition of the untreated and treated lignocellulosic biomass to be monitored [44,45].

The FTIR spectrum of the starting material (Figure 8) shows several signals attributed to the main components of the lignocellulosic biomass (cellulose, hemicellulose and lignin). In particular, the band at 1715 cm^{-1} is associated with the C=O stretching of unconjugated carbonyl groups, whereas the signal at 1370 cm^{-1} is associated with the C-H symmetric deformation that is typical in cellulose and hemicellulose. The band at 1224 cm^{-1} can be attributed to the aryl C-O stretching vibration mode of phenolic hydroxyl groups and is thus assigned to lignin; in addition, the signal at 1260 cm^{-1} is attributed to the methoxy substituents of the aromatic rings in lignin [21,46]. The other weaker bands at 1422 and 1460 cm^{-1} are attributed to the asymmetric component of the C-H deformations in lignin and carbohydrates, respectively. The band at 1508 cm^{-1} is associated with the vibrations of the aromatic C-C skeletons of lignin, the signal at 1158 cm^{-1} is attributed to the C-O-C vibration in cellulose and hemicellulose, and the intense wide peak at 1035 cm^{-1} is associated with the C-O stretching vibrations of cellulose and hemicellulose. The absorption band at 899 cm^{-1} is assigned to the asymmetric C-O-C stretching of the β-(1,4)-glycosidic linkage [44,47].

On the other hand, from the spectrum of the IL-treated sample (Figure 8), many of the peaks associated with the presence of lignin disappear or decrease in intensity, and the peaks characteristic of cellulose and hemicellulose are clearly the predominant peaks. The spectra of the treated samples show an intense absorbance at 1640 cm^{-1} due to the presence of absorbed water. In summary, the FTIR analysis indicates a dramatic change in the chemical composition of the samples after treatment in [EMIM]OAc and subsequent regeneration in presence of acetone:water, which eliminates most of the lignin.

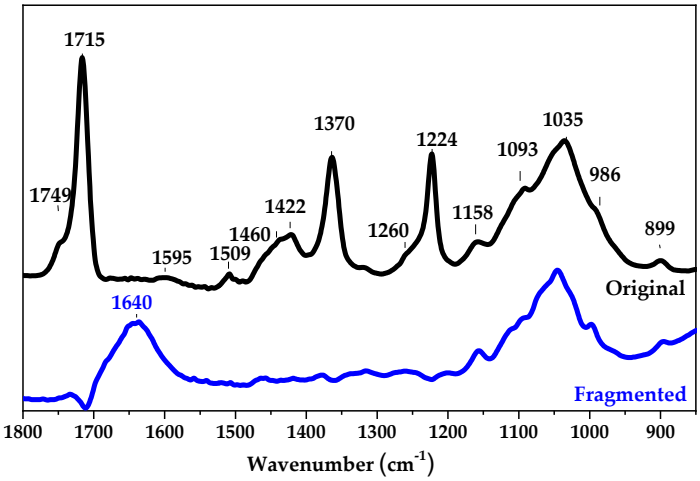

Figure 8. FTIR absorption spectra of the original wheat straw and the solid fraction (rich in sugars) obtained after pretreatment with [EMIM]OAc.

2.7. Catalytic Hydrolysis

To study the effect of the morphology and the presence of additional functional groups on the properties of the catalysts, we compared the reactivity of the AME and AHE catalysts with that of the commercial catalyst Amberlyst 70 in hydrolyzing wheat straw fragmented with [EMIM]OAc. In all the catalytic tests, a suitable amount of the synthesized resin catalyst was employed to keep the concentration of the sulfonic groups constant in the reaction mixture. The changes in the concentration of the main products obtained by hydrolyzing the biomass (glucose, levulinic acid, xylose and furfural) over time are depicted in Figures 9 and 10. Due to the quick decomposition of 5-HMF to levulinic acid in water, the concentration of 5-HMF was generally very low [17]. For this reason, the evolution of the concentration of this product over time is not reported.

Remarkably, the glucose and levulinic acid concentrations are definitely higher in the presence of the AME and AHE copolymers, both gel-type and macroreticular (Figures 9 and 10) than in the presence of the commercial acid catalyst Amberlyst 70. This evidence does not agree with what was expected based on the acid strength of the alkyl and aryl sulfonic groups of the tested catalyst (pKa = 1.9 for propanesulfonic acid; −2.7 for benzenesulfonic acid) [48]. This suggests that the hydroxyl groups (AHE) and carboxylic groups (AME) of the synthetized resins, which are not present in the Amberlyst 70 reference catalyst, act as promoters. Their direct co-catalytic role seems to be ruled out by the relatively low acid strength of the carboxylic and especially of the hydroxyl groups in comparison with the sulfonic groups. For instance, the pK_a of propionic acid, which can be taken as representative of the carboxylic moieties of AME resins, is 4.88 [49] three order of magnitude lower than the pK_a of propanesulfonic acid. In addition, the carboxylic groups of AME resins are lower in amount in comparison with the sulfonic acid groups.

Therefore, the promoting effect of these protic polar groups is likely physico-chemical rather than chemical. On the one hand, their presence could simply affect the hydrophilicity and the swelling behavior in the water of the catalysts, making them more readily accessible to the reactant's molecules. Swelling is of the utmost importance in heterogeneous solid–liquid processes involving cross-linked organic polymers. In this context, a clear difference in the behavior of the AME catalysts can be observed depending on the extent of cross-linking. In particular, the glucose concentration achieved over AME 64-4 and AME 72-4 (gel-type) is higher than that achieved over AME 40-40 and AME 45-40 (macroreticular). Whereas the 4% cross-linked resins are gel-type, the 40% are macroreticular [31,32]. These two classes of polymers differ in many ways; the most important way being their swelling behavior. The gel-type resins are glassy nonporous materials when dry, but, due to the low cross-linking degree, a suitable liquid can permeate the whole polymer framework, making the polymer to completely

swell and thus producing a fully accessible gel-phase that extends throughout the whole volume of the resin. In contrast, the macroreticular resins have permanent mesopores, arising from the partial agglomeration of small, highly cross-linked and dense polymer particles. In this case, only a relatively thin layer of the polymer framework, just beneath the pore walls, can swell. Accordingly, only a small fraction of the polymer framework is involved in forming the accessible gel-phase. This implies that the number of accessible acidic groups per unit of catalyst volume is much higher in the case of sulfonated gel-type resins, which are consequently more catalytically active, than in macroreticular resins. This is somewhat counter-intuitive because macroreticular resins have permanent pores and moderate specific surface areas and are generally believed to be more active catalysts than gel-type resins. However, this simplistic view does not consider that macroreticular resins, due to their relatively high cross-linking degree, have more rigid frameworks, which eventually lower their efficiency and the apparent reaction rate. According to the previous discussion, the generally best performance of the gel-type catalysts investigated herein can be likely attributed to their higher swelling degree. For them, it can be observed that the curves of glucose production are practically superimposed for AHE 64-4 and AHE 72-4 and very close to each other up to 120 min for AME 64-4 and AME 72-4. The promoting effect in the gel-type catalysts, if any, seems little dependent on the OH/SO_3H or $COOH/SO_3H$ ratio. As the catalytic performance of the gel-type resins is the most dependent on the swelling behavior, this implies that for them the OH/SO_3H or $COOH/SO_3H$ ratio has a limited effect on the production of glucose.

To get a deeper insight into the origin of the promoting ability of the hydroxyl and carboxylic groups, macroreticular catalysts can be better compared. The results of AME 40-40 and AME 45-40 not only show that they produce a higher amount of glucose than Amberlyst 70, but also that a higher $COOH/SO_3H$ ratio leads to a higher concentration of glucose. This also true for the gel-type AME 64-4 and AME 72-4 at relatively long reaction time. The beneficial role of polar groups has already been observed in previous works with different heterogeneous catalysts functionalized with sulfonic groups [22] and other polar functional groups [34–38,41]. In some of these examples, the supports were rigid inorganic oxides, whereby effects connected to the swelling of the catalyst do not make sense. Moreover, it has already been reported that in resin catalysts, additional functional groups can favor the adsorption of the reagents with no appreciable increase of their swelling degree ("assisted adsorption"), provided they have some kind of affinity towards the molecules of the reagents. In that case, the "assisted adsorption" was based on hydrophobic interaction [50–52]. It can be therefore argued that also in AME 40-40 and AME 45-40 there is an "assisted adsorption" of the β-(1,4)-glucans sustained by the interactions of their molecules with hydroxyl and carboxylic groups. The effect of the assisted adsorption is to bring to closer contact the β-(1,4)-glucans with the active sulfonic groups or to increase their concentrations nearby the active sites. In view of the polar, protic nature of the hydroxyl and carboxylic groups they most likely interact with β-(1,4)-glucans through hydrogen bonding, in which they can act both as donors or acceptors.

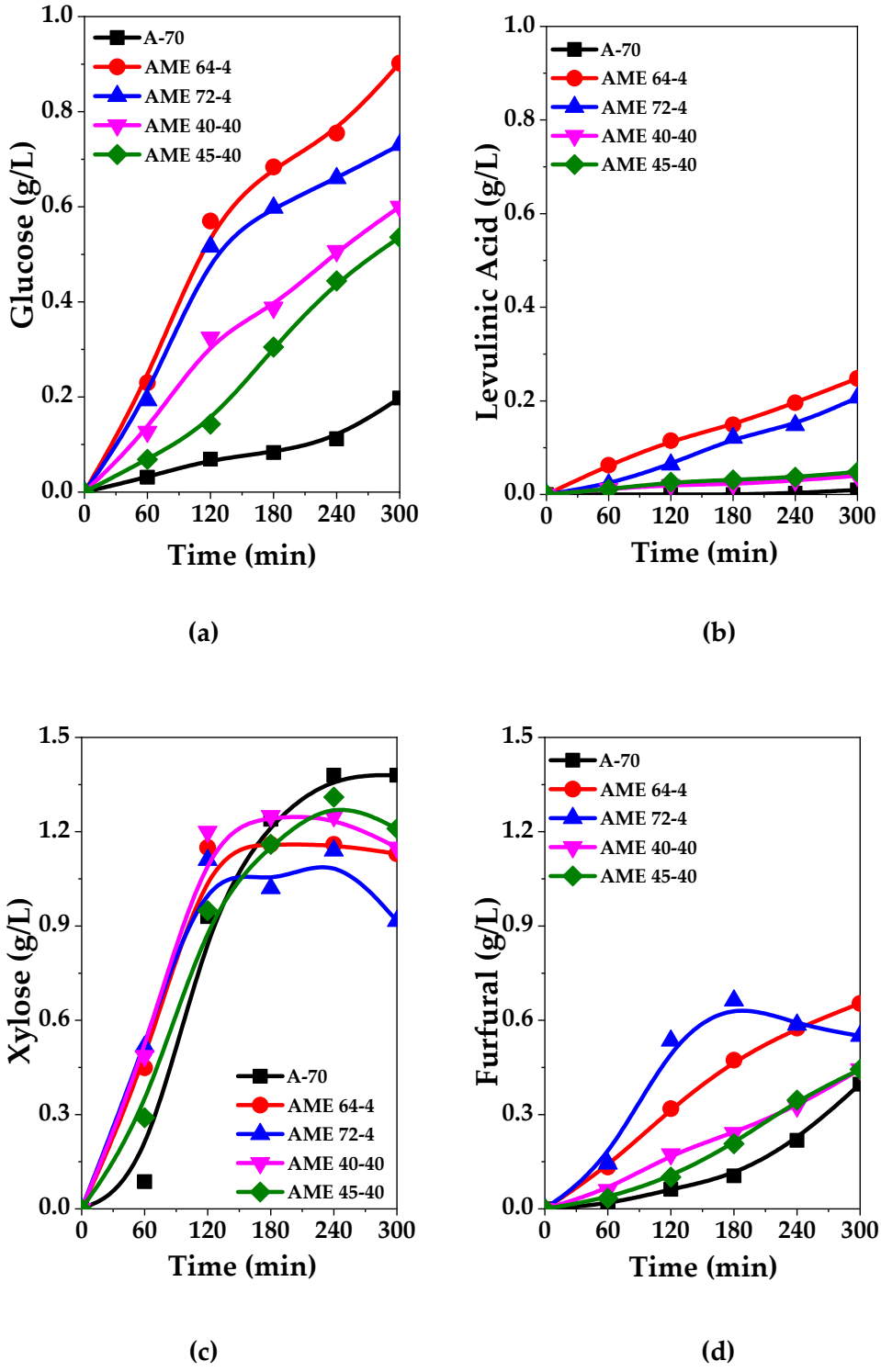

Figure 9. The concentration of (**a**) glucose, (**b**) levulinic acid, (**c**) xylose and (**d**) furfural over time in the hydrolysis of wheat straw catalyzed by the AME materials at 140 °C.

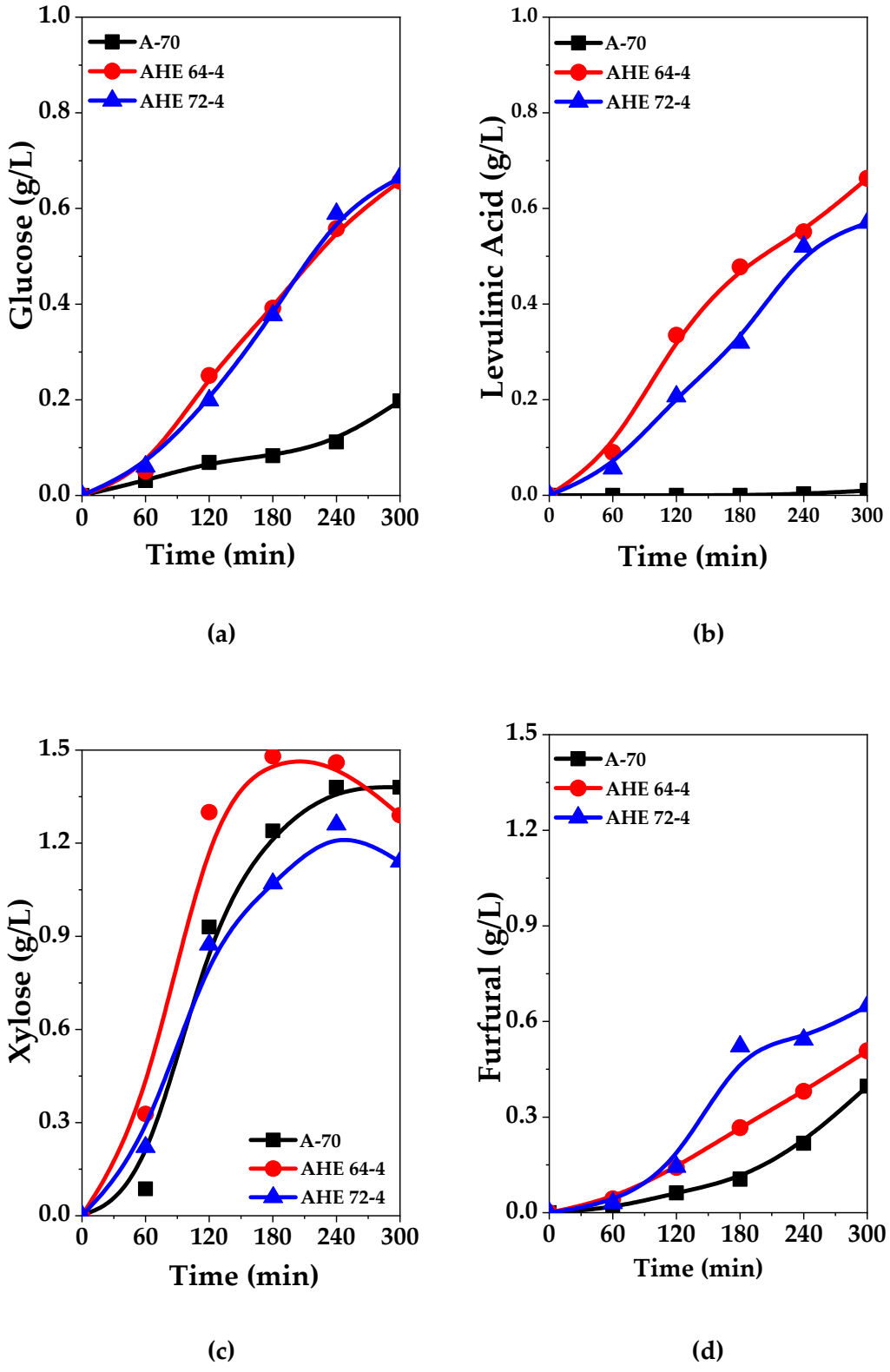

Figure 10. The concentration of (**a**) glucose, (**b**) levulinic acid, (**c**) xylose and (**d**) furfural over time in the hydrolysis of wheat straw catalyzed by the AHE materials at 140 °C.

The concentrations of the products of the hydrolysis of hemicellulose, i.e., xylose and its dehydration product (furfural), are also reported in Figures 9 and 10 as functions of time. The concentration of xylose increases at short reaction times, reaches a maximum and eventually

drops at long reaction times. This can be expected for an intermediate product like xylose, which can be transformed into other products (e.g., furfural) in further consecutive reactions. As expected, the concentration of xylose increases faster than that of glucose, because hemicellulose is easier to hydrolyze than cellulose [5,21,53,54]. This also explains why the concentration of xylose, over time, appears practically independent of the catalyst (including A-70). However, again, the products are generally formed faster over the gel-type catalysts than over the macroreticular catalysts.

3. Materials and Methods

3.1. Materials

Ethylene dimethacrylate (EDMA, Aldrich, St. Louis, MI, USA) and methacrylic acid (MAA, Aldrich, St. Louis, MI, USA) were purified upon distillation prior to use. 2-Acrylamido-2-methyl-1-propane-sulfonic acid (AMPS, Aldrich, St. Louis, MI, USA), 2-hydroxyethyl methacrylate (HEMA, tech grade 97%, Aldrich, St. Louis, MI, USA), azo-bis-isobutyronitrile (AIBN, Janssen Chimica, Beerse, Belgium), dimethylformamide (DMF, Analyticals Carlo Erba, Milano, Italy), methanol (MeOH, Aldrich, St. Louis, MI, USA), sulfuric acid 95%–97% (Aldrich, St. Louis, MI, USA), 1-ethyl-3-methylimidazole acetate ([EMIM]OAc, Aldrich, St. Louis, MI, USA), Avicel cellulose (Fluka Analyticals, Munich, Germany), acetone (Scharlau, Barcelona, Spain), D-(+)-glucose, D-(+)-xylose, 5-hydroxymethylfurfural (5-HMF, Alfa Aesar, Ward Hill, MS, USA), levulinic acid (LA, Aldrich, St. Louis, MI, USA), furfural (Aldrich, St. Louis, MI, USA) and Amberlyst-70 (A-70, Dow chemical, Midland, MI, USA) were used as received. The lignocellulosic biomass (wheat straw) was characterized and supplied by the Unit of Biofuels from the Centre of Energy, Environmental and Technological Research (CIEMAT, Madrid, Spain).

3.2. Synthesis of the AHE Copolymers

Two copolymers containing AMPS, HEMA and EDMA were prepared by adapting the synthetic procedure described by Zecca et al. [55]. The polymers were labeled as AHE Y-X, where Y and Xare the nominal molar ratios of AMPS and the cross-linker (EDMA). AHE 64-4 and AHE 72-4 are characterized by a 4% nominal EDMA molar fraction and a nominal AMPS:HEMA molar ratio of 2:1 and 3:1, respectively. As an example, the procedure used to prepare AHE 64-4 is reported. DMF (10 mL) was added at room temperature to a mixture of AMPS (3.64 g), HEMA (1.14 g), freshly distilled EDMA (0.22 g) and AIBN (0.05 g). The heterogeneous mixture was magnetically stirred at room temperature until AMPS and AIBN were completely dissolved (approximately 30 min). The reaction mixture was held at 70 °C for 72 h. A yellowish solid was obtained. After cooling the system to room temperature, the solid was manually crushed with a steel spatula and swollen in methanol (80 mL) for 3 h. Then, the material was washed with methanol in a Soxhlet extractor for 72 h. The swollen resin was recovered by vacuum filtration and dried for 72 h in a ventilated oven at 70 °C under atmospheric pressure. The resulting yellowish solid was mechanically ground with an impact grinder and sieved to collect the 180–400 μm fraction. The solid was then washed on a column with 1.0 M H_2SO_4 (250 mL) and subsequently washed with distilled water until the filtrate pH was neutral. After vacuum filtration, the solid was dried for 6 days in a ventilated oven at 110 °C under atmospheric pressure. The AHE materials were characterized by elemental analysis, back-titration of the sulfonic groups and FTIR spectroscopy.

3.3. Synthesis of the AME Copolymers

Four copolymers containing AMPS, MAA and EDMA were prepared as reported for the AHE materials, except HEMA was replaced with freshly distilled MAA. The polymers were labeled as AME Y-X, where Y and X are the nominal molar ratios of AMPS and the cross-linker (EDMA). AME 64-4 and AME 72-4 are characterized by a 4% nominal EDMA molar fraction and nominal AMPS:MAA molar ratio of 2:1 and 3:1, respectively. AME 40-40 and AME 45-40 are characterized by a 40% nominal EDMA

molar fraction and a nominal AMPS:MAA molar ratio of 2:1 and 3:1, respectively. The AME materials were characterized by elemental analysis, back-titration of the acidic groups and FTIR spectroscopy.

3.4. Characterization of the Catalysts

The elemental analysis of the catalysts was carried out with a Leco CHNS-932 analyzer. For the back-titration, approximately 100 mg of resin (previously dried at 110 °C in an oven until the weight was constant) was exactly weighed and transferred into a 50 mL Erlenmeyer flask. Then, 10 mL of a 0.1 M NaOH aqueous solution was added. The flask was stoppered and swirled overnight with a mechanical orbiting plate. The next day, the suspension was titrated under magnetic stirring with a standard 0.1 M HCl aqueous solution using a pH-meter equipped with a glass electrode. To assess the potential reaction between NaOH and CO_2 from air, a blank mixture made with 10 mL of the abovementioned 0.1 M NaOH solution was swirled and titrated using the same procedure. The apparent specific content of the sulfonic groups was determined to be the difference of the initial and final millimoles of NaOH (corrected for any overconsumption due to carbonation of the base) divided by the resin mass. Infrared spectra of the catalysts, in absorption mode, were collected with a Bruker Tensor 27 spectrophotometer with KBr pellets. A total of 128 cumulative scans were performed with a resolution of 4 cm^{-1} in the wavenumber range of 4000–400 cm^{-1} in absorption mode.

3.5. Characterization of the Wheat Straw Samples

Raw material (approximately 250 μm particle size) was provided by the Biofuels Unit from the Centre of Energy, Environmental and Technological Research (CIEMAT, Madrid, Spain) and characterized using the National Renewable Energy Laboratory (NREL) standard methods for determining structural carbohydrates and lignin in biomass [21,56] at CIEMAT Biofuels Unit laboratories (Table 3).

Table 3. Composition of the wheat straw samples with respect to the dry weight.

Original Wheat Straw	
Extractives	**12.2 ± 0.7**
Aqueous	9.9 ± 0.4
Organic	1.7 ± 1.22
Monomeric glucose [1]	0.23 ± 0.08
Total glucose [2]	1.04 ± 0.13
Cellulose	**40.1 ± 0.2**
Hemicellulose	**28.6 ± 0.3**
Xylose	24.2 ± 0.2
Galactose	1.6 ± 0.01
Arabinose + Mannose	2.8 ± 0.14
Acid insoluble lignin	**15.4 ± 0.3**
Ashes	**3.6 ± 0.1**
Acetyl groups	**1.6 ± 0.02**

[1] The fraction of monomeric glucose determined in the aqueous extracts after hydrolysis (4% sulfuric acid, 120 °C, 30 min), which was obtained with respect to the dry weight (105 °C). [2] The fraction of monomeric and oligomeric glucose determined in the aqueous extracts after hydrolysis (4% sulfuric acid, 120 °C, 30 min), which was determined with respect to the dry weight (105 °C).

The wheat straw samples before and after pretreatment with [EMIM]OAc were analyzed by X-ray diffraction (XRD, Kassel, Germany), scanning electron microscopy (SEM, Tokyo, Japan) and FTIR spectroscopy (Tokyo, Japan). The XRD diffractograms were recorded using an X'Pert Pro PANalytical diffractometer equipped with a Cu Kα radiation source (λ = 0.15418 nm) and X'Celerator detector that recorded data by Real-Time Multiple Strip (RTMS). After grinding, the samples were placed on a stainless-steel plate. The diffraction patterns were recorded in steps over a range of Bragg

angles (2θ) between 4° and 90° at a scanning rate of 0.02° per step and an accumulation time of 50 s. The diffractograms were analyzed with X'Pert HighScore Plus software (Kassel, Germany).

The scanning electron microscopy (SEM) images of the samples were recorded using a Hitachi S-3000 N microscope. The samples were treated with increasing concentrations of ethanol to fix the structure and dehydrate the samples. After critical-point drying with a Polaron CPD7501 critical point drier, the samples were sputter-coated with a thin layer of gold in a Balzers SCD 004 gold-sputter coater.

The infrared spectra of the wheat straw samples were obtained using Jasco FT/IR-6300 spectrophotometers. The FT-IR spectra were collected in an attenuated total reflectance geometry using a diamond crystal. A total of 180 cumulative scans from 4000–800 cm^{-1} were taken in absorption mode with a resolution of 4 cm^{-1}.

3.6. Wheat Straw Fragmentation

The wheat straw pretreatment was performed in a Mettler Toledo Easy Max 102®reactor equipped with a 100 mL glass vessel, and the samples were mechanically stirred at atmospheric pressure. In a typical pretreatment, 0.5 g of wheat straw was dissolved in 9.5 g of [EMIM]OAc, which had been previously heated at 105 °C under mechanical stirring (500 rpm). The reactor was stoppered, and the mixture was maintained at 105 °C under vigorous mechanical stirring (950 rpm) for 25 min, according to a previous study [6]. A viscous dark brown suspension was obtained. A partially dissolved biomass was regenerated by adding 50 mL of a 1:1 (v/v) water:acetone solution previously cooled in an ice-water bath. The cellulose- and hemicellulose-enriched solid was collected by filtration using a glass fiber filter (pore diameter: 1.6 μm). The wet solid was weighed, and the amount of dry material was determined from the weight loss of an aliquot after drying overnight in an oven at 100 °C.

3.7. Catalytic Tests

The hydrolytic tests were carried out by adapting the optimized procedure for hydrolyzing cellulose as reported by Morales-delaRosa et al. [17]. The tests were performed under magnetic stirring in a 100 mL Teflon-lined steel Berghof reactor equipped with a thermostat, a pressure addition funnel and a tap fitted with a filter, which allowed aliquots to be collected from the reaction mixture free from the solid material.

All the catalytic tests were performed on the fraction that was enriched with polysaccharides, obtainedby precipitating the wheat straw treated with [EMIM]OAc using a water:acetone (1:1) solution for 25 min at 110 °C.

For all the experiments, the amount of catalyst added to the reaction mixture was varied to maintain the sulfonic group concentration at 0.1 M. In a typical run, the heterogeneous catalyst, 0.5 g of wheat straw and 50 mL of water were added, and the suspension was heated to 140 °C. The stirring (500 rpm) and reaction time recording was started when a temperature of 140 °C was attained. Aliquots were periodically withdrawn from the reactor. After 5 h, the reaction was stopped by rapidly cooling the reactor in an ice-water bath (5 min).

3.8. HPLC Analysis

The samples from the reaction mixture were analyzed by HPLC. The monosaccharides (glucose and xylose) were analyzed with an Agilent Technologies 1260 Infinity HPLC (Santa Clara, CA, USA) equipped with an Agilent Technologies Hi-Plex Pb capillary column (300 mm × 7.7 mm) held at 70 °C, and water was used as the mobile phase (0.6 mL/min). Levulinic acid, 5-HMF and furfural were analyzed with an Agilent Technologies 1200 Series HPLC equipped with an Aminex HPX-87H capillary column (300 mm × 7.8 mm) held at 65 °C, and a 0.01 M H_2SO_4 aqueous solution was used as the mobile phase (0.6 mL/min). For the analysis of 5-HMF and furfural, a UV-vis detector (λ = 285 nm) was employed, while the other compounds were analyzed using a refractive index detector. The samples used for the analysis in the 1260 Infinity HPLC were diluted with distilled water (reaction slurry/water

1:1, v:v). The products were identified by comparing their retention times with those of pure reference analytes. The identified compounds were quantified using internal standard calibration curves.

4. Conclusions

The dissolution of wheat straw in [EMIM]OAc and subsequent fractional precipitation with a mixture of acetone:water (1:1) lead to the enrichment of the solid in the polysaccharide fraction, checked by FTIR Spectroscopy. This pretreatment method allows to recover the IL in the filtrate liquid avoiding the presence of [EMIM]OAc in the following steps and rendering the process more economically attractive.

This methodology allows to make the wheat straw surface much more accessible to an acid catalyst. The XRD pattern of the treated wheat straw indicated that it was noncrystalline, and SEM micrographs showed that the original structure disappeared after IL-pretreatment.

Sulfonic resins functionalized with polar groups in addition to -SO_3H groups (AHE and AME) are more effective catalysts in the hydrolytic process than Amberlyst 70. In the case of the gel-type catalysts (AHE 72-4, AHE 64-4, AME 72-4 and AME 64-4) this could be simply the result of their higher swelling degree, which makes a larger fraction of active sites accessible to the molecules of the reagents. This highlights the importance of the morphology of the catalyst and its swelling ability when it is a cross-linked organic resin and is used under liquid–solid conditions. However, it can be also argued that the alcoholic hydroxyl groups and carboxylic groups in the polymer framework of the AHE and AME catalysts, respectively, speed up the breakdown of the β-(1,4) glycosidic bonds by favoring the adsorption of glucans ("assisted adsorption") through hydrogen bonding. This effect seems particularly relevant in the macroreticular catalysts (AME 40-40, AME 45-40).

In addition, the morphology of the catalysts appears to be crucial in terms of glucose production. Gel-type catalysts had the highest glucose concentration, as a larger number of the catalytic sites were accessible to the substrate.

The use of heterogeneous catalysts in the hydrolysis of lignocellulosic materials is a difficult topic because it involves an interaction between two solids. In this way, some different approaches have been studied, firstly the modification of the lignocellulosic materials increasing their accessibility and favoring the contact with catalysts, and the second approach beingthe use of the catalysts supports with polar groups that favor the adsorption of cellulose chains increasing the interaction with the acid site. In this work, we add a step forward, using catalysts functionalized with some polar groups, but also showing the importance of the morphology of the catalysts (gel-type or macroreticular), to enhance the interaction with carbohydrate substrates, mainly cellulose chains. Summing up, this manuscript combines all three approaches, pretreatment of lignocellulosic biomass, catalysts with polar groups and morphology of the catalysts, and the results showed opens the way to design new and efficient heterogeneous catalysts for the hydrolysis of lignocellulosic biomass.

Author Contributions: S.M.-d. designed the experiments. G.L. and S.M.-d. wrote the manuscript. J.M.C.-M. and P.C. designed the experiments and reviewed the manuscript. G.L. and S.M.-d. performed the experimental analyses. J.L.G.F. and M.Z. critically reviewed the manuscript.

Funding: This research was funded by Comunidad de Madrid (Spain), grant numbers S2013/MAE-2882 (RESTOENE-2-CM) and P2018/EMT-4344 (BIOTRES-CM), and the University of Padova under project CPDA123471.

Conflicts of Interest: The authors declare that the research was conducted in the absence of any commercial or financial relationships that could be construed as a potential conflict of interest.

References

1. García-Condado, S.; López-Lozano, R.; Panarello, L.; Cerrani, I.; Nisini, L.; Zucchini, A.; Van der Velde, M.; Baruth, B. Assessing lignocellulosic biomass production from crop residues in the European Union: Modelling, analysis of the current scenario and drivers of interannual variability. *GCB Bioenergy* **2019**. [CrossRef]
2. Scarlat, N.; Dallemand, J.-F.; Monforti-Ferrario, F.; Nita, V. The role of biomass and bioenergy in a future bioeconomy: Policies and facts. *Environ. Dev.* **2015**, *15*, 3–34. [CrossRef]

3. Instituto para la Diversificación y ahorro de la Energía. *Plan de Energías Renovables 2011–2020*; IDAE: Madrid, Spain, 2011.
4. Malins, S.S.A.C. *Availability of Cellulosic Residues and Wastes in the Eu*; The International Council on Clean Transportation: Washington, DC, USA, 2013; White Paper.
5. Alvira, P.; Tomas-Pejo, E.; Ballesteros, M.; Negro, M.J. Pretreatment technologies for an efficient bioethanol production process based on enzymatic hydrolysis: A review. *Bioresour. Technol.* **2010**, *101*, 4851–4861. [CrossRef] [PubMed]
6. Lara-Serrano, M.; Morales-delaRosa, S.; Campos-Martín, M.J.; Fierro, L.J. Fractionation of Lignocellulosic Biomass by Selective Precipitation from Ionic Liquid Dissolution. *Appl. Sci.* **2019**, *9*, 1862. [CrossRef]
7. Zhang, Y.H.P.; Ding, S.Y.; Mielenz, J.R.; Cui, J.B.; Elander, R.T.; Laser, M.; Himmel, M.E.; McMillan, J.R.; Lynd, L.R. Fractionating recalcitrant lignocellulose at modest reaction conditions. *Biotechnol. Bioeng.* **2007**, *97*, 214–223. [CrossRef]
8. Lan, W.; Liu, C.F.; Sun, R.C. Fractionation of bagasse into cellulose, hemicelluloses, and lignin with ionic liquid treatment followed by alkaline extraction. *J. Agric. Food. Chem.* **2011**, *59*, 8691–8701. [CrossRef] [PubMed]
9. da Costa Lopes, A.M.; João, K.G.; Rubik, D.F.; Bogel-Łukasik, E.; Duarte, L.C.; Andreaus, J.; Bogel-Łukasik, R. Pre-treatment of lignocellulosic biomass using ionic liquids: Wheat straw fractionation. *Bioresour. Technol.* **2013**, *142*, 198–208. [CrossRef]
10. Yang, D.; Zhong, L.-X.; Yuan, T.-Q.; Peng, X.-W.; Sun, R.-C. Studies on the structural characterization of lignin, hemicelluloses and cellulose fractionated by ionic liquid followed by alkaline extraction from bamboo. *Ind. Crop. Prod.* **2013**, *43*, 141–149. [CrossRef]
11. Yang, X.; Wang, Q.; Yu, H. Dissolution and regeneration of biopolymers in ionic liquids. *Russ. Chem. Bull.* **2014**, *63*, 555–559. [CrossRef]
12. Zhang, P.; Dong, S.J.; Ma, H.H.; Zhang, B.X.; Wang, Y.F.; Hu, X.M. Fractionation of corn stover into cellulose, hemicellulose and lignin using a series of ionic liquids. *Ind. Crop. Prod.* **2015**, *76*, 688–696. [CrossRef]
13. Morais, A.R.C.; Pinto, J.V.; Nunes, D.; Roseiro, L.B.; Oliveira, M.C.; Fortunato, E.; Bogel-Łukasik, R. Imidazole: Prospect Solvent for Lignocellulosic Biomass Fractionation and Delignification. *ACS Sustain. Chem. Eng.* **2016**, *4*, 1643–1652. [CrossRef]
14. Mohtar, S.S.; Tengku Malim Busu, T.N.; Md Noor, A.M.; Shaari, N.; Mat, H. An ionic liquid treatment and fractionation of cellulose, hemicellulose and lignin from oil palm empty fruit bunch. *Carbohydr. Polym.* **2017**, *166*, 291–299. [CrossRef] [PubMed]
15. Zhou, C.-H.; Xia, X.; Lin, C.-X.; Tong, D.-S.; Beltramini, J. Catalytic conversion of lignocellulosic biomass to fine chemicals and fuels. *Chem. Soc. Rev.* **2011**, *40*, 5588–5617. [CrossRef] [PubMed]
16. Geboers, J.A.; Van de Vyver, S.; Ooms, R.; Op de Beeck, B.; Jacobs, P.A.; Sels, B.F. Chemocatalytic conversion of cellulose: Opportunities, advances and pitfalls. *Catal. Sci. Tech.* **2011**, *1*, 714. [CrossRef]
17. Morales-delaRosa, S.; Campos-Martin, J.M.; Fierro, J.L.G. Optimization of the process of chemical hydrolysis of cellulose to glucose. *Cellulose* **2014**, *21*, 2397–2407. [CrossRef]
18. Li, C.; Wang, Q.; Zhao, Z.K. Acid in ionic liquid: An efficient system for hydrolysis of lignocellulose. *Green Chem.* **2008**, *10*, 177. [CrossRef]
19. Morales-delaRosa, S.; Campos-Martin, J.M.; Fierro, J.L.G. High glucose yields from the hydrolysis of cellulose dissolved in ionic liquids. *Chem. Eng. J.* **2012**, *181–182*, 538–541. [CrossRef]
20. Padrino, B.; Lara-Serrano, M.; Morales-delaRosa, S.; Campos-Martín, J.M.; Fierro, J.L.G.; Martínez, F.; Melero, J.A.; Puyol, D. Resource Recovery Potential From Lignocellulosic Feedstock Upon Lysis with Ionic Liquids. *Front. Bioeng. Biotechnol.* **2018**, 6. [CrossRef]
21. Lara-Serrano, M.; Sáez Angulo, F.; Negro, M.J.; Morales-delaRosa, S.; Campos-Martin, J.M.; Fierro, J.L.G. Second-Generation Bioethanol Production Combining Simultaneous Fermentation and Saccharification of IL-Pretreated Barley Straw. *ACS Sustain. Chem. Eng.* **2018**, *6*, 7086–7095. [CrossRef]
22. Morales-delaRosa, S.; Campos-Martin, J.M.; Fierro, J.L.G. Chemical hydrolysis of cellulose into fermentable sugars through ionic liquids and antisolvent pretreatments using heterogeneous catalysts. *Catal. Today* **2018**, *302*, 87–93. [CrossRef]
23. Fukuoka, A.; Dhepe, P.L. Catalytic Conversion of Cellulose into Sugar Alcohols. *Angew. Chem. Int. Ed.* **2006**, *45*, 5161–5163. [CrossRef] [PubMed]

24. Onda, A.; Ochi, T.; Yanagisawa, K. Selective hydrolysis of cellulose into glucose over solid acid catalysts. *Green Chem.* **2008**, *10*, 1033. [CrossRef]
25. Vilcocq, L.; Castilho, P.C.; Carvalheiro, F.; Duarte, L.C. Hydrolysis of Oligosaccharides Over Solid Acid Catalysts: A Review. *ChemSusChem* **2014**, *7*, 1010–1019. [CrossRef] [PubMed]
26. Biasi, P.; Mikkola, J.P.; Sterchele, S.; Salmi, T.; Gemo, N.; Shchukarev, A.; Centomo, P.; Zecca, M.; Canu, P.; Rautio, A.R.; et al. Revealing the role of bromide in the H2O2 direct synthesis with the catalyst wet pretreatment method (CWPM). *AlChE J.* **2017**, *63*, 32–42. [CrossRef]
27. Centomo, P.; Meneghini, C.; Sterchele, S.; Trapananti, A.; Aquilanti, G.; Zecca, M. EXAFS in situ: The effect of bromide on Pd during the catalytic direct synthesis of hydrogen peroxide in memory of the late Professor Benedetto Corain (July 8th 1941–September 24th 2014), passionate chemist and teacher. *Catal. Today* **2015**, *248*, 138–141. [CrossRef]
28. Centomo, P.; Zecca, M.; Di Noto, V.; Lavina, S.; Bombi, G.G.; Nodari, L.; Salviulo, G.; Ingoglia, R.; Milone, C.; Galvagno, S.; et al. Characterization of Synthetic Iron Oxides and their Performance as Support for Au Catalysts. *ChemCatChem* **2010**, *2*, 1143–1149. [CrossRef]
29. Centomo, P.; Zecca, M.; Zoleo, A.; Maniero, A.L.; Canton, P.; Jeřábek, K.; Corain, B. Cross-linked polyvinyl polymersversus polyureas as designed supports for catalytically active M0 nanoclusters Part III. Nanometer scale structure of the cross-linked polyurea support EnCat 30 and of the PdII/EnCat 30 and Pd0/EnCat 30NP catalysts. *Phys. Chem. Chem. Phys.* **2009**, *11*, 4068–4076. [CrossRef] [PubMed]
30. Sterchele, S.; Centomo, P.; Zecca, M.; Hanková, L.; Jeřábek, K. Dry- and swollen-state morphology of novel high surface area polymers. *Microporous Mesoporous Mater.* **2014**, *185*, 26–29. [CrossRef]
31. Kennedy, F.R. Syntheses and separations using functional polymers. *Br. Polym. J.* **1989**, *21*, 359–360. [CrossRef]
32. Zecca, M.; Centomo, P.; Corain, B. Metal Nanoclusters Supported on Cross-Linked Functional Polymers: A Class of Emerging Metal Catalysts. In *Metal Nanoclusters in Catalysis and Materials Science: The Issue of Size Control*; Elsevier: Amsterdam, The Netherlands, 2008; pp. 201–232. [CrossRef]
33. Jeřábek, K.; Hanková, L.; Holub, L. Working-state morphologies of ion exchange catalysts and their influence on reaction kinetics. *J. Mol. Catal. A Chem.* **2010**, *333*, 109–113. [CrossRef]
34. Suganuma, S.; Nakajima, K.; Kitano, M.; Yamaguchi, D.; Kato, H.; Hayashi, S.; Hara, M. Hydrolysis of Cellulose by Amorphous Carbon Bearing SO3H, COOH, and OH Groups. *J. Am. Chem. Soc.* **2008**, *130*, 12787–12793. [CrossRef] [PubMed]
35. Pang, J.; Wang, A.; Zheng, M.; Zhang, T. Hydrolysis of cellulose into glucose over carbons sulfonated at elevated temperatures. *Chem. Commun.* **2010**, *46*, 6935–6937. [CrossRef] [PubMed]
36. Foo, G.S.; Sievers, C. Synergistic Effect between Defect Sites and Functional Groups on the Hydrolysis of Cellulose over Activated Carbon. *ChemSusChem* **2015**, *8*, 534–543. [CrossRef] [PubMed]
37. Huang, Y.-B.; Fu, Y. Hydrolysis of cellulose to glucose by solid acid catalysts. *Green Chem.* **2013**, *15*, 1095. [CrossRef]
38. Van de Vyver, S.; Peng, L.; Geboers, J.; Schepers, H.; de Clippel, F.; Gommes, C.J.; Goderis, B.; Jacobs, P.A.; Sels, B.F. Sulfonated silica/carbon nanocomposites as novel catalysts for hydrolysis of cellulose to glucose. *Green Chem.* **2010**, *12*, 1560–1563. [CrossRef]
39. Morales-delaRosa, S.; Campos-Martin, J.M.; Fierro, J.L.G. Complete Chemical Hydrolysis of Cellulose into Fermentable Sugars through Ionic Liquids and Antisolvent Pretreatments. *ChemSusChem* **2014**, *7*, 3467–3475. [CrossRef] [PubMed]
40. Li, X.; Jiang, Y.; Shuai, L.; Wang, L.; Meng, L.; Mu, X. Sulfonated copolymers with SO3H and COOH groups for the hydrolysis of polysaccharides. *J. Mater. Chem.* **2012**, *22*, 1283–1289. [CrossRef]
41. Silverstein, R.M.; Webster, F.X.; Kiemle, D.J. *Spectrometric Identification of Organic Compounds*, 7th ed.; Wiley: Hoboken, NJ, USA, 2005.
42. Park, S.; Baker, J.O.; Himmel, M.E.; Parilla, P.A.; Johnson, D.K. Cellulose crystallinity index: Measurement techniques and their impact on interpreting cellulase performance. *Biotechnol. Biofuels* **2010**, *3*, 10. [CrossRef]
43. Wang, H.; Gurau, G.; Pingali, S.V.; O'Neill, H.M.; Evans, B.R.; Urban, V.S.; Heller, W.T.; Rogers, R.D. Physical Insight into Switchgrass Dissolution in Ionic Liquid 1-Ethyl-3-methylimidazolium Acetate. *ACS Sustain. Chem. Eng.* **2014**, *2*, 1264–1269. [CrossRef]
44. Pandey, K.K.; Pitman, A.J. FTIR studies of the changes in wood chemistry following decay by brown-rot and white-rot fungi. *Int. Biodeterior. Biodegrad.* **2003**, *52*, 151–160. [CrossRef]

45. Osatiashtiani, A.; Lee, A.F.; Granollers, M.; Brown, D.R.; Olivi, L.; Morales, G.; Melero, J.A.; Wilson, K. Hydrothermally Stable, Conformal, Sulfated Zirconia Monolayer Catalysts for Glucose Conversion to 5-HMF. *ACS Catal.* **2015**, *5*, 4345–4352. [CrossRef]
46. Hergert, H.L. Infrared Spectra of Lignin and Related Compounds. II. Conifer Lignin and Model Compounds 1,2. *J. Org. Chem.* **1960**, *25*, 405–413. [CrossRef]
47. Sun, R.C.; Fang, J.M.; Tomkinson, J.; Geng, Z.C.; Liu, J.C. Fractional isolation, physico-chemical characterization and homogeneous esterification of hemicelluloses from fast-growing poplar wood. *Carbohydr. Polym.* **2001**, *44*, 29–39. [CrossRef]
48. Buckingham, J.; Cadogan, J.D.G.; Raphael, R.A.; Rees, C.W. *Dictionary of Organic Compounds*, 5th ed.; Chapman and Hall: New York, NY, USA, 1982.
49. Serjeant, E.P.; Dempsey, B. *Ionisation Constants of Organic Acids in Aqueous Solution*; IUPAC Chemical Data Series No. 23; Pergamon Press, Inc.: New York, NY, USA, 1979.
50. Martinuzzi, S.; Cozzula, D.; Centomo, P.; Zecca, M.; Müller, T.E. The distinct role of the flexible polymer matrix in catalytic conversions over immobilised nanoparticles. *Rsc Adv.* **2015**, *5*, 56181–56188. [CrossRef]
51. Centomo, P.; Bonato, I.; Hanková, L.; Holub, L.; Jeřábek, K.; Zecca, M. Novel Ion-Exchange Catalysts for Reactions Involving Lipophilic Reagents: Perspectives in the Reaction of Esterifications of Fatty Acids with Methanol. *Top. Catal.* **2013**, *56*, 611–617. [CrossRef]
52. Jerabek, K.H.L.; Holub, L.; Corain, B.; Zecca, M.; Centomo, P.; Bonato, I. Strongly Acidic Ion Exchanger Catalyst and Method of Preparing The Same. WO2012127414, 27 september 2012.
53. Morales-Delarosa, S.; Campos-Martin, J.M. 6—Catalytic processes and catalyst development in biorefining. In *Advances in Biorefineries*; Waldron, K., Ed.; Woodhead Publishing: Cambridge, UK, 2014; pp. 152–198. [CrossRef]
54. Kumar, P.; Barrett, D.M.; Delwiche, M.J.; Stroeve, P. Methods for Pretreatment of Lignocellulosic Biomass for Efficient Hydrolysis and Biofuel Production. *Ind. Eng. Chem. Res.* **2009**, *48*, 3713–3729. [CrossRef]
55. Centomo, P.; Jeřábek, K.; Canova, D.; Zoleo, A.; Maniero, A.L.; Sassi, A.; Canton, P.; Corain, B.; Zecca, M. Highly Hydrophilic Copolymers of N,N-Dimethylacrylamide, Acrylamido-2-methylpropanesulfonic acid, and Ethylenedimethacrylate: Nanoscale Morphology in the Swollen State and Use as Exotemplates for Synthesis of Nanostructured Ferric Oxide. *Chem. A Eur. J.* **2012**, *18*, 6632–6643. [CrossRef]
56. Sluiter, J.B.; Ruiz, R.O.; Scarlata, C.J.; Sluiter, A.D.; Templeton, D.W. Compositional analysis of lignocellulosic feedstocks. 1. Review and description of methods. *J. Agric. Food. Chem.* **2010**, *58*, 9043–9053. [CrossRef]